crystals

MDPI

Article

The Effect of Titanium Oxyfluoride Morphology on Photocatalytic Activity of Fluorine-Doped Titanium(IV) Oxide

Marta Kowalkińska [1,*], Jakub Karczewski [2] and Anna Zielińska-Jurek [1,*]

[1] Department of Process Engineering and Chemical Technology, Gdansk University of Technology, Gabriela Narutowicza 11/12, 80-233 Gdansk, Poland
[2] Institute of Nanotechnology and Materials Engineering, Faculty of Applied Physics and Mathematics, Gdansk University of Technology, Gabriela Narutowicza 11/12, 80-233 Gdansk, Poland
* Correspondence: marta.kowalkinska@pg.edu.pl (M.K.); annjurek@pg.edu.pl (A.Z.-J.)

Abstract: Titanium oxyfluoride ($TiOF_2$) is a metastable product that can be obtained in a fluorine-rich environment. This material can also be a valuable precursor in the synthesis of titanium(IV) oxide (TiO_2). However, the effect of $TiOF_2$ morphology on the physicochemical properties of TiO_2 has not been studied so far. In this work, single-phase $TiOF_2$ was prepared by a solvothermal method. The as-synthesized samples exhibited a variety of morphologies, including different shapes and crystallite sizes. These materials were characterized by X-ray diffraction (XRD), scanning electron microscopy (SEM) combined with energy-dispersive X-ray spectroscopy (EDS), surface area measurements, thermal gravimetric analysis (TGA) and UV–vis diffuse reflectance spectroscopy (DR/UV–vis). Furthermore, $TiOF_2$ samples were used as precursors in the synthesis of fluorine-doped titanium(IV) oxide and applied in photocatalytic phenol degradation under UV-vis light. The experiments showed that the crystallite size of the precursor, as well as the number of fluoride ions used in the synthesis, were the predominant factors that affected the photocatalytic activity of the final photocatalyst.

Keywords: titanium oxyfluoride; morphology; titanium(IV) oxide; nanostructures; photocatalyst; phenol degradation

Citation: Kowalkińska, M.; Karczewski, J.; Zielińska-Jurek, A. The Effect of Titanium Oxyfluoride Morphology on Photocatalytic Activity of Fluorine-Doped Titanium(IV) Oxide. *Crystals* **2023**, *13*, 356. https://doi.org/10.3390/cryst13020356

Academic Editor: Dah-Shyang Tsai

Received: 2 February 2023
Revised: 14 February 2023
Accepted: 16 February 2023
Published: 19 February 2023

1. Introduction

Titanium oxyfluoride ($TiOF_2$) is a semiconducting material that exists in two polymorphs: a cubic structure and a hexagonal unit cell, which is thermodynamically less favoured [1]. $TiOF_2$ can be easily synthesized by a solvothermal route, usually with the addition of hydrofluoric acid [2–4]. Titanium oxyfluoride has been mainly investigated as an electrode material for lithium-ion batteries. The utilization of this compound could have numerous advantages, including air stability and low hygroscopicity [5]. According to Reddy et al., $TiOF_2$ with a cubic unit cell can intercalate four lithium atoms, while the accident-related energy capacity is higher than commercially available graphite nodes [6]. Nanostructured titanium oxyfluoride is also advantageous due to its more developed surface area, larger pore volume, and shorter diffusion path for ion transport than its macroscopic counterparts [5,7]. Therefore, further research on $TiOF_2$-based materials may be useful in terms of electrochemical applications.

Recently, $TiOF_2$ has also been proposed as a photocatalytic material in heterogeneous photocatalysis. However, this material does not actually demonstrate noticeable photocatalytic activity, as has been studied in H_2 evolution [8], hydroxyl radicals generation [9] and decomposition of organic pollutants so far [10,11]. Due to low photocatalytic activity and limited practical application, titanium oxyfluoride is still overlooked in the literature. However, in some studies, $TiOF_2$ is proposed as a precursor of titanium(IV) oxide (TiO_2), which is one of the most described and characterized photocatalysts in the literature [12–15]. Our recent studies showed that the hydrothermal treatment of $TiOF_2$ in the presence of capping agents allowed us to obtain anatase nanostructures or fluorine-doped TiO_2 nanocrystals,

with exposed {1 0 1}, {0 0 1} and {1 0 0} facets [4,16]. Therefore, considering the practical aspect of $TiOF_2$ utilization as a precursor, further investigation of this material is needed.

It is well known that the morphology of the material is a key factor that may influence either the photocatalytic performance or electrochemical properties [17–19]. However, the morphological design of the material may be applied to both the final product as well as the precursor. To our best knowledge, there are no studies concerning the $TiOF_2$ morphologies' effect on the final structure and properties of TiO_2-based materials. Therefore, the main aim of the present study was the design and synthesis of $TiOF_2$ with a desired structure, including HF-assisted and acid-free synthesis and physicochemical characterization of $TiOF_2$ samples. Furthermore, fluorine-doped TiO_2 from different $TiOF_2$ precursors was characterized and applied in photocatalytic phenol degradation under simulated solar light.

2. Materials and Methods

The synthesis of titanium oxyfluoride was proceeded via a solvothermal route. Titanium(IV) fluoride (TiF_4), titanium(IV) isopropoxide (TTIP), 1-butanol, hydrofluoric acid 48% (HF), acetic acid (CH_3COOH), ammonium fluoride (NH_4F) and ammonia water 25% ($NH_{3(aq)}$) were provided by Chemat, Poland.

2.1. Synthesis of Titanium Oxyfluoride and F-Modified Titanium(IV) Oxide

In a typical procedure of $TiOF_2$ synthesis, TiF_4 or TTIP are used as precursors. The samples obtained from TTIP are denoted as TP, whereas materials originating from TiF_4 are labeled as TF. In the case of TF series, the labels are completed by the volume of hydrofluoric acid used in the synthesis. The detailed parameters of synthesis conditions and the nomenclature are presented in Table 1 and the subsections below.

Table 1. Synthesis conditions and nomenclature of $TiOF_2$ samples.

Sample Name	Titanium Source	Titanium Source Amount	Solvent	Solvent Volume (cm^3)	HF Volume (cm^3)	Reaction Temperature and Time
TP	TTIP	10.2 cm^3	CH_3COOH	24.4	3.9	200 °C, 12 h
TF_0HF	TiF_4	10 g	1-butanol	120	-	210 °C, 24 h
TF_0.085HF		3.06 g			0.085	
TF_0.17HF					0.17	

2.1.1. Synthesis of $TiOF_2$–TP Series

The demonstrated synthesis of $TiOF_2$ was based on Chen et al., with modifications [20]. The appropriate amount of TTIP was mixed with acetic acid and kept under stirring using a Teflon-coated magnetic stirrer bar at room temperature. After 15 min, HF was slowly added and stirring was continued for 15 min. The obtained mixture was then transferred into a 200 cm^3 Teflon-lined stainless-steel autoclave and heated at 200 °C for 12 h. The obtained product was separated through centrifugation and washed several times thoroughly with ethanol and deionized water to remove the residual organic contamination. After drying at 80 °C overnight, the TP sample was harvested.

2.1.2. Synthesis of $TiOF_2$–TF Series

TF_0HF sample was synthesized using TiF_4 powder, which was added into a 200 cm^3 Teflon reactor with 120 cm^3 of 1-butanol. The obtained mixture was stirred for 30 min to form a uniform suspension. Furthermore, the reactor was transferred into a stainless-steel autoclave immediately and heated at 210 °C for 24 h. The obtained product was separated through centrifugation and washed several times with ethanol and deionized water. Finally, the grey powder was dried at 80 °C overnight.

A similar procedure was applied to obtain samples TF_0.085HF and TF_0.17HF, but a different mass of TiF_4 was used. In addition, after forming the stable suspension, the

desired amount of HF was slowly injected. After this step, the reactor was transferred into an autoclave immediately.

2.1.3. Synthesis of Fluorine-Modified TiO_2

Fluorine-modified photocatalysts were synthesized using $TiOF_2$ as precursors. In this regard, 0.2 g $TiOF_2$ sample was dispersed in 45 cm^3 of deionized water (DI). Simultaneously, 0.2904 g NH_4F was dissolved in 45 cm^3 DI. NH_4F solution was added to $TiOF_2$ mixture and stirred for 15 min using a magnetic stirrer. Next, 10 cm^3 of ammonia water was added to the mixture and the stirring was continued for 15 min. The obtained mixture was transferred into a 200 cm^3 Teflon-lined stainless-steel autoclave and kept at 200 °C for 20 h and then cooled down naturally. After each reaction, beige precipitates were centrifuged and washed several times with DI and ethanol to remove residual inorganic ions, then dried at 80 °C overnight.

2.2. Materials Characterization

The crystal structure of the samples and phase identification were investigated by X-ray powder diffraction (Rigaku MiniFlex 600 X-Ray diffractometer, Tokyo, Japan) with Cu Kα radiation. Data were collected in a 2θ range of 5°–80° with a scan speed 1° min^{-1} and scan steps 0.01°. The analysis and Rietveld refinements were performed with the HighScore Plus software package (Malvern Panalytical, Malvern, United Kingdom) and the Crystallography Open Database, with data fitting based on the pseudo-Voigt profile function. Several parameters were refined, i.e., the specimen displacement, lattice parameters, polynomial coefficients for the background function, profile parameters and Gaussian and Lorentzian profile coefficients. The estimation of the crystallite size was performed on the basis of Scherrer's equation. A field emission scanning electron microscope (SEM, FEI Quanta FEG 250, Hillsboro, OR, USA) was used to determine the morphologies of $TiOF_2$ samples. The presence of titanium and fluorine in all powders was confirmed by energy-dispersive X-ray spectroscopy (EDS). The Brunauer–Emmett–Teller (BET) surface area of $TiOF_2$ and F-TiO_2 samples was measured by nitrogen adsorption using a Micromeritics Gemini V instrument. All powders were degassed at 200 °C for 120 min prior to N_2 adsorption measurements. The BET surface area was determined by a multipoint BET method. To study the absorption properties, diffuse reflectance UV−visible spectra (DRS/UV−vis) were measured using a Thermo Fisher Scientific Evolution 220 spectrophotometer. Barium sulfate was used as a reflectance standard. Based on the obtained data, bandgap energy (E_g) calculations were performed using Tauc's method. To study the thermal stability and phase transition of $TiOF_2$, thermal gravimetric analyses (TGA) were performed using Thermal Analysis System 2 SF/1100 (Mettler Toledo, Greifensee, Switzerland). The measurements were performed in a range of 25–800 °C at a heating rate of 10 °C·min^{-1} under a nitrogen atmosphere.

2.3. Photocatalytic Phenol Degradation

The photocatalytic activity of F-TiO_2 photocatalysts was tested towards phenol degradation under UV-vis light, performed in a black box. In a typical experiment, 25 cm^3 of 20 mg·dm^{-3} phenol solution and 25 mg of the photocatalyst were put into a quartz reactor under magnetic stirring with a speed of 800 rpm. The suspension was aerated with a constant airflow of 5 dm^3·h^{-1}. For an experiment, a 300 W xenon lamp was used as simulated solar light. The UV spectrum flux intensity at the reactor border was set as 45 mW·cm^{-2}. Before irradiation, the whole system was kept in darkness for 30 min to provide the adsorption−desorption equilibrium. After that, the process was initiated by turning on the xenon lamp. The liquid samples (1.0 cm^3) were collected every 15 min and filtered through syringe filters (pore size = 0.2 μm) to remove the photocatalyst particles.

The phenol concentration was monitored using a high-performance liquid chromatography system (HPLC, model Shimadzu LC-6A, Kyoto, Japan), combined with a photodiode array detector (SPD-M20A) and a C18 column (Phenomenex Gemini 5 μm; 150 × 4.6 mm,

California, USA) working at a temperature of 45 °C. During measurements, the mobile phase, composed of (*v*/*v*) 70% acetonitrile, 29.5% water and 0.5% orthophosphoric acid, was used at a flow rate of 0.3 $cm^3 \cdot min^{-1}$. HPLC-grade acetonitrile, orthophosphoric acid solution and phenol were provided by Merck. Quantitative phenol analysis was performed using standard compounds using the external calibration method.

3. Results and Discussion

3.1. Structural and Morphological Analyses of $TiOF_2$

To confirm the presence of titanium oxyfluoride in the as-synthesized samples, powder X-Ray Diffraction (XRD) was performed. XRD patterns of investigated materials compared with the calculated model are presented in Figure 1. The experimental XRD patterns of the obtained samples were compared with the reference card 01-077-0132. The presence of the $TiOF_2$ phase with cubic structure and space group Pm-3 m is observed in all samples. The unit cell parameters from Rietveld refinement are presented in Table 2. No additional peaks, as well as low χ^2 as a parameter of the goodness of fit, indicated that the obtained samples are single phase. Moreover, the crystallite size estimated using Scherrer's equation is in a range of 40–49 nm in all cases.

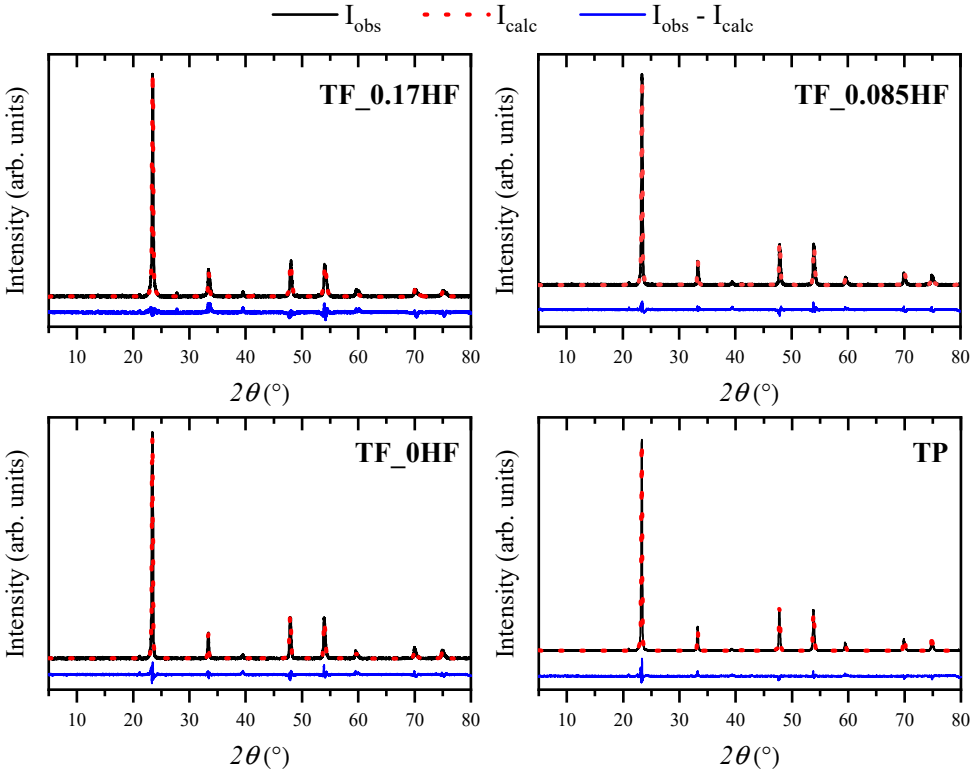

Figure 1. XRD patterns of synthesized $TiOF_2$ samples.

Table 2. Lattice and microstructural parameters of $TiOF_2$ obtained by XRD, BET and EDS analysis.

Sample Name	Crystallite Size (nm)	F/Ti Ratio Calculated from EDS Spectroscopy	Surface Area S_{BET} ($m^2 \cdot g^{-1}$)	Lattice Parameters $a = b = c$ (Å)	Goodness of Fit χ^2
TP	49	2.19	3.9	3.799	1.89
TF_0HF	43	2.13	5.2	3.794	1.48
TF_0.085HF	44	2.08	8.5	3.796	1.37
TF_0.17HF	40	-	-	3.788	2.62

The morphologies of $TiOF_2$ powders were further studied using scanning electron microscopy analysis. Figure 2 shows SEM images of the as-synthesized samples. Comparing

all the SEM images, the difference in morphology within obtained powders was distinct. The sample TF_0.17HF (Figure 2a) exhibited large agglomerates with a solid structure and smooth surface, in which smaller crystallites cannot be unambiguously distinguished. Within the solid structure, square-shaped openings can be observed. In contrast to this solid morphology, in the case of sample TF_0.085HF (Figure 2b), small particles with undefined shapes can be observed. This variation is in agreement with the literature because increased fluoride ion concentrations promote the growth of large particles [4,21]. However, solvothermal alcoholysis of TiF_4 without HF addition (Figure 2c) led to the formation of a mixture of cubic and spherical particles. The morphology is not uniform, which is probably due to the high amount of TiF_4 precursor with respect to 1-butanol. According to Wang et al., an oxidation process to $TiOF_2$ results from hydrolysis of the initially formed $(RO)_xTiF_{4-x}$ complex. At this stage, the particles are spherical and the further prolongation of solvothermal synthesis allows one to shape transformation to cubes [10]. A distinct cubic shape was noticed in the TP sample (Figure 2d). An addition of acetic acid was probably responsible for two effects: support in HF-assisted crystal growth and a factor determining the morphology [22].

In general, titanium oxyfluoride can undergo hydrolysis under air conditions and transform into anatase [23]. In this regard, theoretically, $TiOF_2$ should be stored under low humic conditions. However, only TF_0.17HF from the series, when stored in the presence of air, starts oxidizing to titanium(IV) oxide. In other cases, this reaction does not occur, and these samples are stable. The probable explanation of this phenomenon is the high Ti/F ratio used in the synthesis. The solvothermal route with TiF_4 and HF is also the method of synthesizing TiO_2 with exposed {0 0 1} facets [21,24]. Therefore, an increased F^- amount at the material's surface may promote the hydrolysis and formation of TiO_2.

Finally, EDS spectroscopy was used to estimate the presence of fluorine in $TiOF_2$ samples. Based on these results, the average atomic F/Ti ratio was calculated (see Table 2). These values are close to the theoretical F/Ti ratio from the general formula of titanium oxyfluoride, which equals 2.0.

Furthermore, the surface area analyses (S_{BET}) using the BET method for $TiOF_2$ samples were performed. The S_{BET} values are presented in Table 2. All powders possessed a surface area below 10 $m^2 \cdot g^{-1}$. The lowest S_{BET} value was observed for the TP sample, which can be explained by the high amount of hydrofluoric acid used in the synthesis and, in consequence, the largest crystallite size. Although in the preparation of TF series, titanium fluoride was used as a precursor, the absence or low amount of HF was probably responsible for the small crystallite size of $TiOF_2$ and increasing the surface area compared to the TP sample.

The optical properties, including light absorption, were determined using diffuse-reflectance (DR) UV-Vis spectroscopy. The DR/UV-vis spectra of as-prepared titanium oxyfluoride samples are presented in Figure 3. All samples possessed the highest absorbance in a range of 200–400 nm, which is similar to TiO_2 [25,26]. Moreover, all samples in the series were capable of absorbing light above 400 nm, which is in accordance with the fact that these powders are gray. Based on the transformation of the Kubelka–Munk function, the bandgap energies of titanium oxyfluoride samples were calculated. The E_g values equaled 3.2–3.3 eV, which is consistent with previous reports [2,4].

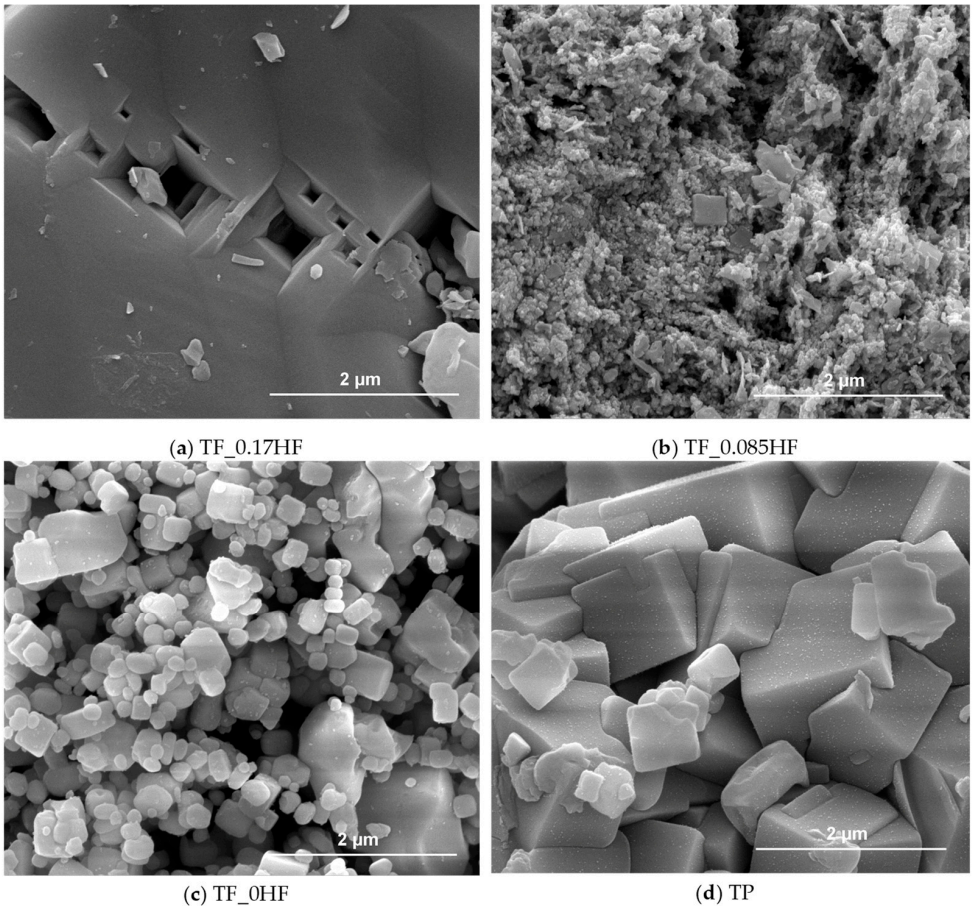

Figure 2. SEM images of as-prepared samples.

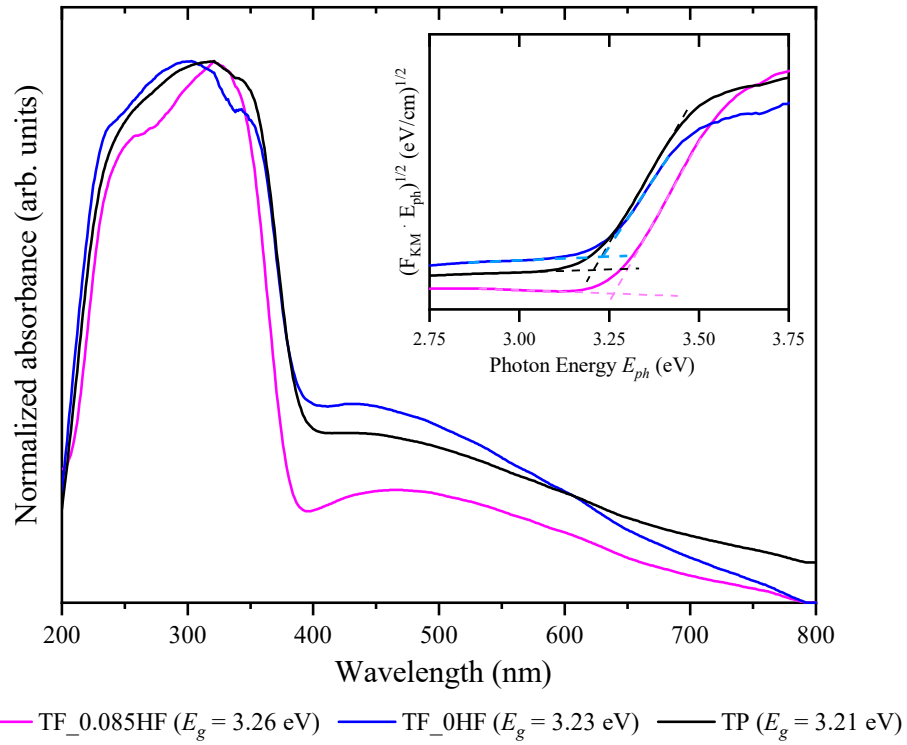

Figure 3. DR/UV-vis spectra of obtained $TiOF_2$. The inset shows the transformation of Kubelka–Munk function vs. photon energy.

For a better characterization of the thermal stability of titanium oxyfluoride samples, thermal gravimetry analyses (TGA) were performed. The TGA curves are presented in Figure 4. A distinct weight loss is observed at a temperature of around 550 °C in the case of all three samples. The mass variations at these temperatures are −45.17%, −46.75% and −48.16% for samples TP, TF_0HF and TF_0.085HF, respectively. These results showed that under a nitrogen atmosphere, $TiOF_2$ does not transform into TiO_2 directly; theoretically, in that case, the mass loss should achieve a value around c.a. −32%. According to Xie et al., the following transition may occur: 2 $TiOF_2 \rightarrow TiO_2 + TiF_4$ [27]. However, these measurements were performed under air conditions, whereas our samples were heated under a non-oxidizing atmosphere. Moreover, the powders after TGA analyses had a dark-blue-gray color, but X-ray diffraction confirmed the presence of anatase. Therefore, this phase transition may be more complex. The probable explanation is that weight loss results from $TiOF_2$ transformation to the Ti-O Magneli phase [28]. This product is apparently metastable and undergoes oxidation to anatase under air conditions. However, based on the powder color, the final material would be defective and oxygen deficient [25].

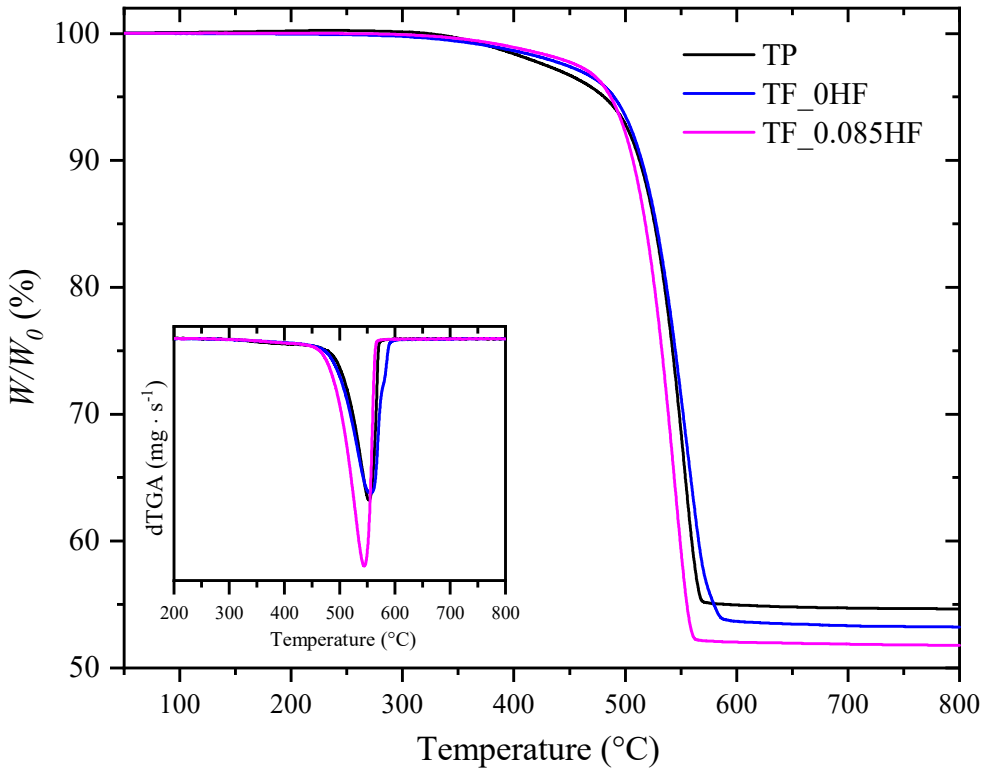

Figure 4. TGA curves of $TiOF_2$ samples. The inset shows the first derivative dTGA in relation to temperature.

3.2. Characterization and Photocatalytic Activity of TiO_2 Synthesized from $TiOF_2$

To study the effect of precursor morphology on the final photocatalyst properties, X-ray diffraction analyses were performed. The XRD patterns of F-TiO_2 are presented in Figure 5. The experimental XRD pattern of the obtained photocatalysts was compared with the reference card 03-065-5714. Each $TiOF_2$ precursor was successfully transformed to anatase under hydrothermal conditions. Moreover, comparing the crystallite size of anatase samples (Table 3) with the values from Table 2, it can be noticed that the transformation from titanium oxyfluoride to titanium(IV) oxide allows photocatalysts with small crystallite size to be achieved. Specifically, sample TP, which exhibited the largest crystallite size in the $TiOF_2$ series, was able to synthesize F-TiO_2 with the smallest crystallites. Finally, the presence of fluorine in the photocatalysts was confirmed by EDS spectroscopy. The results of the average F/Ti ratio for F-TiO_2 are presented in Table 3.

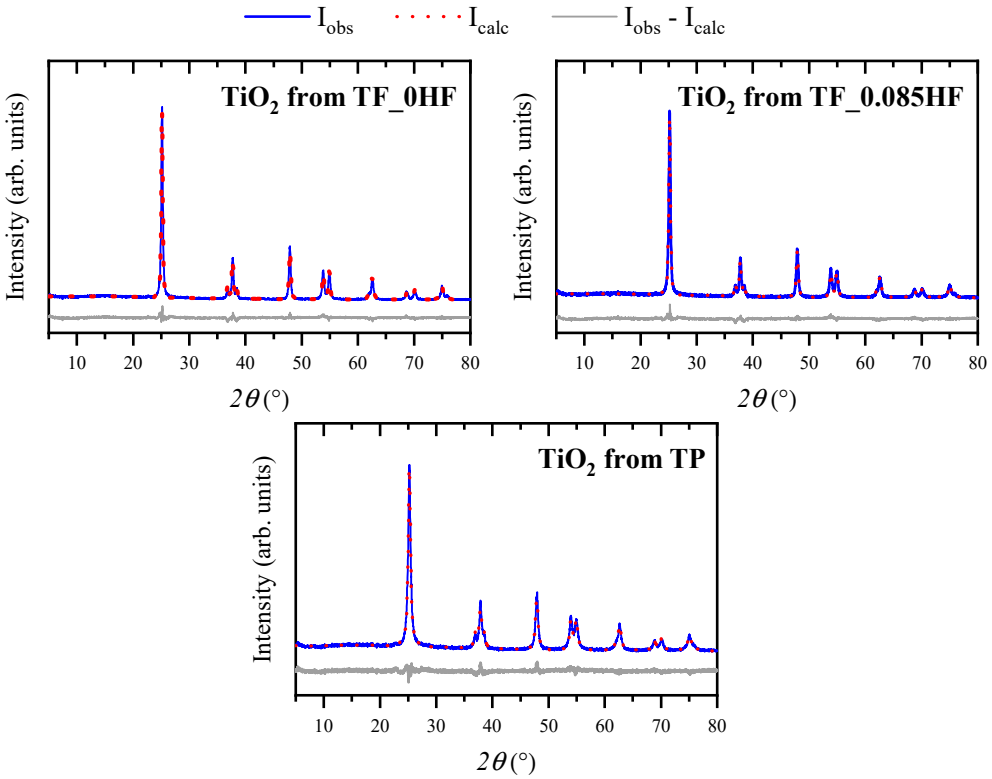

Figure 5. XRD patterns of F-modified TiO_2.

Table 3. Lattice and microstructural parameters of F-TiO_2 obtained by XRD, BET and EDS analysis.

Sample Name	Crystallite Size (nm)	F/Ti Ratio Calculated from EDS Spectroscopy	Surface Area S_{BET} ($m^2 \cdot g^{-1}$)	Lattice Parameter $a = b$ (Å)	Lattice Parameter c (Å)	Goodness of Fit χ^2
TiO_2 from TP	17	0.086	38.9	3.793	9.488	1.94
TiO_2 from TF_0HF	28	0.072	20.7	3.786	9.499	2.05
TiO_2 from TF_0.085HF	24	0.054	28.1	3.788	9.497	1.95

The differences in crystallite size between samples are correlated with the specific surface area, which is an important factor concerning the improvement in photocatalytic activity [29]. Therefore, to complete the characterization of F-TiO_2 samples, surface area measurements using the BET method were performed. The highest surface area of 38.9 $m^2 \cdot g^{-1}$ was observed in TiO_2 obtained from TP, although this precursor exhibited the lowest surface area in the $TiOF_2$ samples. However, these measurements are consistent with the estimated crystallite size by Scherrer's equation. In the case of the photocatalysts synthesized from precursors in the TF series, S_{BET} values of about 21–28 $m^2 \cdot g^{-1}$ were noticed.

Finally, the photocatalytic degradation of phenol under UV-vis light in the presence of F-TiO_2 was determined. The changes in phenol concentration during the photocatalytic process are presented in Figure 6a. Under these conditions, the effect of photolysis was negligible. All F-TiO_2 samples were capable of degrading phenol under simulated solar light. However, the reaction rate constants (Figure 6b) differed for particular photocatalysts. The lowest phenol degradation efficiency was observed for TiO_2 prepared from TP; this is the only sample that did not fully degrade phenol after 60 min of the photocatalytic process. For this photocatalytic process, the main phenol derivative detected by HPLC-DAD was 1,2-dihydroxybenzene (catechol). Remarkably, TiO_2 from TP was supposed to have the smallest crystallite size in the anatase series, but according to SEM images, the

formed cubes were bigger than crystallites in TF_0HF and TF_0.085HF. Moreover, these photocatalysts exhibited the highest surface area in the F-TiO_2 series. Meanwhile, the application of the TF series as precursors allowed us to achieve almost 100% degradation of initial phenol concentration after 1 h of irradiation. For both photocatalytic processes, two phenol derivatives were predominant: catechol and benzene-1,4-diol (hydroquinone). It is worth highlighting that the precursor TF_0HF was the only sample in which, during solvothermal synthesis, no hydrofluoric acid was used. For this photocatalyst, the highest reaction rate constant was noticed. No correlation between either specific surface area of fluorinated anatase or the atomic F/Ti was observed. The more important factor was the morphology of the precursors; $TiOF_2$ from the TF series exhibited smaller crystallite size and higher surface area than the TP sample. The crystallite size and surface area depended on the F^- content in the solvothermal reaction. Therefore, we can conclude that $TiOF_2$ precursor morphology primarily influences the photocatalytic activity of the anatase-based photocatalytic material. In particular, the crystallite size and the number of fluoride ions used in the synthesis significantly influenced the efficiency of phenol degradation.

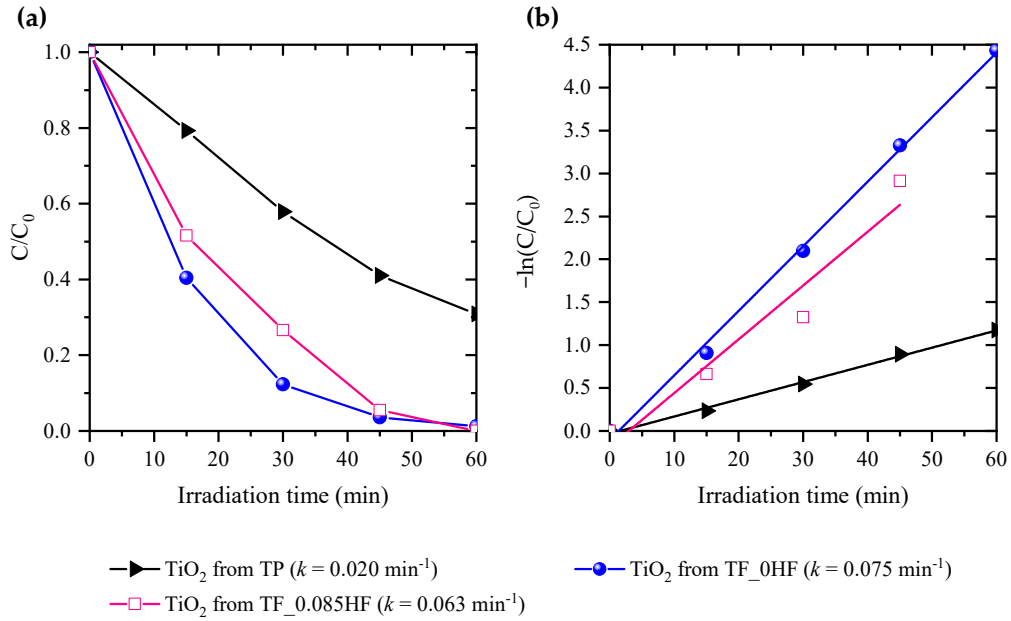

Figure 6. Photocatalytic degradation of phenol as a function of concentration to initial concentration (**a**) and $ln(C/C_0)$ (**b**).

Previously, it was reported that the morphology of the photocatalysts affects their photocatalytic activity. Our recent studies about anatase nanostructures with exposed crystal facets showed that facet exposition was responsible for photocatalytic activity as well as naproxen and phenol degradation pathways [4,16]. The role of morphology was also investigated by Sulowska et al., who studied organic–inorganic photocatalysts consisting of two-dimensional anatase nanosheets modified with PEDOT [30]. Various PEDOT morphologies were obtained, including; globular, stuck spindles and microvesicular structures. It was found that the highest photocatalytic hexavalent chromium removal was observed for 2D TiO_2 combined with microvesicular PEDOT.

Next to photocatalysts' morphology, a vital role of the substrate type used in photocatalyst synthesis was also described in certain studies. For example, in the synthesis of anatase nanocrystals with exposed {0 0 1} facets, the aliphatic chain length in alcohol solvent influenced the crystal growth rate and the final morphology of TiO_2 [25,31]. Next to the solvent type, it was found that the precursor used in the photocatalyst's preparation can affect the properties of the final product. This effect was comprehensively studied by Li et al., who investigated octahedral anatase nanostructures with exposed {1 0 1} facets [32]. A two-step synthesis was performed to obtain these nanocrystals with defined morphology,

where the titanium source was potassium titanate nanowires. It was found that an ion exchange between potassium and ammonium cations influenced the transformation mechanism to titanium(IV) oxide; instead of the in-site transformation and topochemical reaction, a dissolution–nucleation process was predominant. Therefore, the synthesis of TiO_2 with well-defined facets was more controllable. The effect of the precursor was also described by Xia et al., who investigated graphitic carbon nitride for photocatalytic H_2 evolution [33]. To obtain different g-C_3N_4 photocatalysts, thermal polycondensation syntheses using guanidine hydrochloride, melamine, urea, dicyandiamide and thiourea as the precursors were performed. Among the obtained photocatalysts, g-C_3N_4 synthesized from urea possessed the most desirable morphology, including the porous-layered structure and high specific surface area. The above examples showed that the morphology of the precursor is an important factor that should be considered when designing a new photocatalyst with desirable properties.

4. Conclusions

In this work, a facile approach to synthesize titanium oxyfluoride ($TiOF_2$) with different morphologies was developed. The solvothermal route was proposed to obtain this metastable material using TTIP or TiF4 as precursors and, optionally, HF as a reagent and capping agent. X-ray diffraction supported by Rietveld refinements confirmed the presence of single-phase materials. Based on electron microscopy analysis, various morphologies were confirmed, including different shapes and crystallite sizes. However, in most cases, the microstructure of titanium oxyfluoride had no influence on the thermal stability. The fluorine content in all samples and atomic F/Ti ratio determined by EDS spectroscopy were close to the theoretical F/Ti ratio from the general formula of titanium oxyfluoride. Thermal gravimetric analysis curves showed a distinct weight loss at a temperature of about 550 °C, which can be attributed to the formation of the oxygen-deficient oxide. Finally, these samples were applied in the synthesis of fluorine-doped titanium(IV) oxide. The hydrothermal conditions allowed us to complete $TiOF_2$ transformation to anatase with a small crystallite size and high surface area. These materials were applied for photocatalytic phenol degradation under simulated solar light. The analyses showed that F-TiO_2 prepared from the precursor TF_0HF exhibited the highest photocatalytic activity in the series. Surprisingly, the smallest crystallite size of the fluorinated anatase and high specific surface area did not influence phenol degradation efficiency under UV-vis light. Therefore, we supposed that the final photocatalytic activity depended on the crystallite size of titanium oxyfluoride and the number of fluoride ions used in the synthesis of the precursor. It can also be assumed that the morphology of the precursor is a crucial parameter affecting the final photocatalytic material physicochemical properties and should be worthy of attention in further investigations.

Author Contributions: Conceptualization, M.K. and A.Z.-J.; methodology, M.K. and A.Z.-J.; validation, M.K. and A.Z.-J.; formal analysis, M.K. and J.K.; investigation, M.K. and A.Z.-J.; writing—original draft preparation, M.K.; writing—review and editing, M.K. and A.Z.-J.; supervision, A.Z.-J.; project administration, A.Z.-J.; funding acquisition, A.Z.-J. All authors have read and agreed to the published version of the manuscript.

Funding: This research was funded by the Polish National Science Centre, contract No. UMO-2021/43/B/ST5/02983.

Institutional Review Board Statement: Not applicable.

Informed Consent Statement: Not applicable.

Data Availability Statement: The authors confirm that the data supporting the findings of this study are available within the article. Derived data supporting the findings of this study are available from the corresponding author [A.Z.-J.] on request.

Conflicts of Interest: The authors declare no conflict of interest.

References

1. Shian, S.; Sandhage, K.H. Hexagonal and Cubic $TiOF_2$. *J. Appl. Crystallogr.* **2010**, *43*, 757–761. [CrossRef]
2. Lu, Y.; Yan, H.; Huang, E.; Chen, B. Persistent Negative Compressibility Coupled to Optical Modulation in Empty-Perovskite $TiOF_2$. *J. Phys. Chem. C* **2021**, *125*, 8869–8875. [CrossRef]
3. Wang, Z.; Yu, K.; Feng, Y.; Qi, R.; Ren, J.; Zhu, Z. Stabilizing Ti3C2Tx-MXenes with $TiOF_2$ Nanospheres Intercalation to Improve Hydrogen Evolution Reaction and Humidity-Sensing Performance. *Appl. Surf. Sci.* **2019**, *496*. [CrossRef]
4. Kowalkińska, M.; Dudziak, S.; Karczewski, J.; Ryl, J.; Trykowski, G.; Zielińska-Jurek, A. Facet Effect of TiO_2 Nanostructures from $TiOF_2$ and Their Photocatalytic Activity. *Chemical. Eng. J.* **2021**, *404*, 126493. [CrossRef]
5. Louvain, N.; Karkar, Z.; El-Ghozzi, M.; Bonnet, P.; Guérin, K.; Willmann, P. Fluorination of Anatase TiO_2 towards Titanium Oxyfluoride $TiOF_2$: A Novel Synthesis Approach and Proof of the Li-Insertion Mechanism. *J. Mater. Chem. A Mater.* **2014**, *2*, 15308–15315. [CrossRef]
6. Reddy, M.V.; Madhavi, S.; Subba Rao, G.V.; Chowdari, B.V.R. Metal Oxyfluorides $TiOF_2$ and NbO_2F as Anodes for Li-Ion Batteries. *J. Power Sour.* **2006**, *162*, 1312–1321. [CrossRef]
7. Jung, M.J.; Kim, Y.; Lee, Y.S. Enhancement of the Electrochemical Capacitance of $TiOF_2$obtained via Control of the Crystal Structure. *J. Ind. Eng. Chem.* **2017**, *47*, 187–193. [CrossRef]
8. Wen, C.Z.; Hu, Q.H.; Guo, Y.N.; Gong, X.Q.; Qiao, S.Z.; Yang, H.G. From Titanium Oxydifluoride ($TiOF_2$) to Titania (TiO_2): Phase Transition and Non-Metal Doping with Enhanced Photocatalytic Hydrogen (H2) Evolution Properties. *Chem. Commun.* **2011**, *47*, 6138–6140. [CrossRef]
9. Wang, Z.; Lv, K.; Wang, G.; Deng, K.; Tang, D. Study on the Shape Control and Photocatalytic Activity of High-Energy Anatase Titania. *Appl. Catal. B* **2010**, *100*, 378–385. [CrossRef]
10. Wang, J.; Cao, F.; Bian, Z.; Leung, M.K.H.; Li, H. Ultrafine Single-Crystal $TiOF_2$ Nanocubes with Mesoporous Structure, High Activity and Durability in Visible Light Driven Photocatalysis. *Nanoscale* **2014**, *6*, 897–902. [CrossRef]
11. Lv, K.; Yu, J.; Cui, L.; Chen, S.; Li, M. Preparation of Thermally Stable Anatase TiO_2 Photocatalyst from $TiOF_2$ Precursor and Its Photocatalytic Activity. *J. Alloy. Compd.* **2011**, *509*, 4557–4562. [CrossRef]
12. Lv, K.; Guo, X.; Wu, X.; Li, Q.; Ho, W.; Li, M.; Ye, H.; Du, D. Photocatalytic Selective Oxidation of Phenol to Produce Dihydroxybenzenes in a TiO2/UV System: Hydroxyl Radical versus Hole. *Appl. Catal. B* **2016**, *199*, 405–411. [CrossRef]
13. Dalton, J.S.; Janes, P.; Jones, N.; Hallam, K.R.; Nicholson, J.A.; Allen, G.C. Photocatalytic Oxidation of NOx Gases Using TiO_2: A Spectroscopic Approach. *Environ. Pollut.* **2002**, *45120*, 415–422. [CrossRef] [PubMed]
14. Sobczyński, A.; Duczmal, L.; Zmudziński, W. Phenol Destruction by Photocatalysis on TiO_2: An Attempt to Solve the Reaction Mechanism. *J. Mol. Catal. A Chem.* **2004**, *213*, 225–230. [CrossRef]
15. Rej, S.; Hejazi, S.M.H.; Badura, Z.; Zoppellaro, G.; Kalytchuk, S.; Kment, Š.; Fornasiero, P.; Naldoni, A. Light-Induced Defect Formation and Pt Single Atoms Synergistically Boost Photocatalytic H2 Production in 2D TiO_2-Bronze Nanosheets. *ACS Sustain. Chem. Eng.* **2022**, *10*, 17286–17296. [CrossRef]
16. Kowalkińska, M.; Sikora, K.; Łapiński, M.; Karczewski, J.; Zielińska-Jurek, A. Non-Toxic Fluorine-Doped TiO2 Nanocrystals from $TiOF_2$ for Facet-Dependent Naproxen Degradation. *Catal. Today* **2022**. [CrossRef]
17. Nakata, K.; Fujishima, A. TiO_2 Photocatalysis: Design and Applications. *J. Photochem. Photobiol. C Photochem. Rev.* **2012**, *13*, 169–189. [CrossRef]
18. Zhang, Y.; Deng, B.; Zhang, T.; Gao, D.; Xu, A.W. Shape Effects of Cu_2O Polyhedral Microcrystals on Photocatalytic Activity. *J. Phys. Chem. C* **2010**, *114*, 5073–5079. [CrossRef]
19. Mazierski, P.; Sowik, J.; Miodyńska, M.; Trykowski, G.; Mikołajczyk, A.; Klimczuk, T.; Lisowski, W.; Nadolna, J.; Zaleska-Medynska, A. Shape-Controllable Synthesis of GdVO4 Photocatalysts and Their Tunable Properties in Photocatalytic Hydrogen Generation. *Dalton Trans.* **2019**, *48*, 1662–1671. [CrossRef]
20. Chen, L.; Shen, L.; Nie, P.; Zhang, X.; Li, H. Facile Hydrothermal Synthesis of Single Crystalline $TiOF_2$ Nanocubes and Their Phase Transitions to TiO_2 Hollow Nanocages as Anode Materials for Lithium-Ion Battery. *Electrochim Acta* **2012**, *62*, 408–415. [CrossRef]
21. Wen, C.Z.; Zhou, J.Z.; Jiang, H.B.; Hu, Q.H.; Qiao, S.Z.; Yang, H.G. Synthesis of Micro-Sized Titanium Dioxide Nanosheets Wholly Exposed with High-Energy {001} and {100} Facets. *Chem. Commun.* **2011**, *47*, 4400–4402. [CrossRef] [PubMed]
22. Ye, J.; Liu, W.; Cai, J.; Chen, S.; Zhao, X.; Zhou, H.; Qi, L. Nanoporous Anatase TiO_2 Mesocrystals: Additive-Free Synthesis, Remarkable Crystalline-Phase Stability, and Improved Lithium Insertion Behavior. *J. Am. Chem. Soc.* **2011**, *133*, 933–940. [CrossRef] [PubMed]
23. Wang, L.; Liu, J.; Min, Y.; Zhang, K. Nontopological Transformation of Hierarchical TiO_2 by Self-Regulated Etching and Capping Roles of F—For Photocatalytic H 2 Evolution. *Appl. Surf. Sci.* **2019**, *473*, 738–745. [CrossRef]
24. Gordon, T.R.; Cargnello, M.; Paik, T.; Mangolini, F.; Weber, R.T.; Fornasiero, P.; Murray, C.B. Nonaqueous Synthesis of TiO_2 Nanocrystals Using TiF4 to Engineer Morphology, Oxygen Vacancy Concentration, and Photocatalytic Activity. *J. Am. Chem. Soc.* **2012**, *134*, 6751–6761. [CrossRef] [PubMed]
25. Dudziak, S.; Kowalkińska, M.; Karczewski, J.; Pisarek, M.; Siuzdak, K.; Kubiak, A.; Siwińska-Ciesielczyk, K.; Zielińska-Jurek, A. Solvothermal Growth of {0 0 1} Exposed Anatase Nanosheets and Their Ability to Mineralize Organic Pollutants. The Effect of Alcohol Type and Content on the Nucleation and Growth of TiO_2 Nanostructures. *Appl. Surf. Sci.* **2021**, *563*, 150360. [CrossRef]

26. Kumar, M.M.; Badrinarayanan, S.; Sastry, M. Nanocrystalline TiO_2 Studied by Optical, FTIR and X-Ray Photoelectron Spectroscopy: Correlation to Presence of Surface States. *Thin Solid Film.* **2000**, *358*, 122–130. [CrossRef]
27. Xie, S.; Han, X.; Kuang, Q.; Fu, J.; Zhang, L.; Xie, Z.; Zheng, L. Solid State Precursor Strategy for Synthesizing Hollow TiO_2 Boxes with a High Percentage of Reactive {001} Facets Exposed. *Chem. Commun.* **2011**, *47*, 6722–6724. [CrossRef]
28. Okamoto, H. O-Ti (Oxygen-Titanium). *J. Phase Equilibria Diffus* **2011**, *32*, 473–474. [CrossRef]
29. Song, G.; Gao, R.; Zhao, Z.; Zhang, Y.; Tan, H.; Li, H.; Wang, D.; Sun, Z.; Feng, M. High-Spin State Fe(III) Doped TiO_2 for Electrocatalytic Nitrogen Fixation Induced by Surface F Modification. *Appl. Catal. B* **2022**, *301*. [CrossRef]
30. Sulowska, A.; Fiszka Borzyszkowska, A.; Cysewska, K.; Siwińska-Ciesielczyk, K.; Nikiforow, K.; Trykowski, G.; Zielińska-Jurek, A. The Effect of PEDOT Morphology on Hexavalent Chromium Reduction over 2D TiO_2/PEDOT Photocatalyst under UV–Vis Light. *Mater. Chem. Phys.* **2023**, 127430. [CrossRef]
31. Zheng, Y.; Wang, J.; Yang, P. Anatase TiO_2 Nanosheets Exposed {001} Facet: Solvent Effects on the Photocatalytic Performance. *J. Nanosci. Nanotechnol.* **2017**, *17*, 1204–1209. [CrossRef] [PubMed]
32. Li, J.; Yu, Y.; Chen, Q.; Li, J.; Xu, D. Controllable Synthesis of TiO_2 Single Crystals with Tunable Shapes Using Ammonium-Exchanged Titanate Nanowires as Precursors. *Cryst. Growth Des.* **2010**, *10*, 2111–2115. [CrossRef]
33. Xia, P.; Li, G.; Li, X.; Yuan, S.; Wang, K.; Huang, D.; Ji, Y.; Dong, Y.; Wu, X.; Zhu, L.; et al. Synthesis of G-C3N4 from Various Precursors for Photocatalytic H2 Evolution under the Visible Light. *Crystals* **2022**, *12*, 1719. [CrossRef]